Effect of nano-yttria stabilized zirconia addition on the microstructure and mechanical properties of Ti6Al4V parts manufactured by selective laser melting

Amine Hattal, Thierry Chauveau, Madjid Djemai, Jean Jacques Fouchet, Brigitte Bacroix, Guy Dirras

Materials and Design 180 (2019) 107909

Contents lists available at ScienceDirect

Materials and Design

journal homepage: www.elsevier.com/locate/matdes

Effect of nano-yttria stabilized zirconia addition on the microstructure and mechanical properties of Ti6Al4V parts manufactured by selective laser melting

Amine Hattal [a,b], Thierry Chauveau [a], Madjid Djemai [b], Jean Jacques Fouchet [b], Brigitte Bacroix [a], Guy Dirras [a,*]

[a] Université Paris 13, LSPM-CNRS, 99 avenue Jean Baptiste Clément, 932430 Villetaneuse, France
[b] Z3Dlab, Parc Technologique, 26 Rue des Sablons, Montmagny 95360, France

HIGHLIGHTS

- Homogenous powder blend of Ti6Al4V and nYSZ was obtained.
- β peaks in SLMed parts were only found after addition of 1% and 2.5% of nYSZ to Ti6Al4V.
- Residual stress decrease shifted Ti6Al4V HT, XRD peaks toward lower angles.
- Microhardness increased from 340 to 511 HV with nYSZ addition to Ti6Al4V matrix.
- Addition of 1% of nYSZ to Ti6Al4V increased the compression strength without ductility loss.

GRAPHICAL ABSTRACT

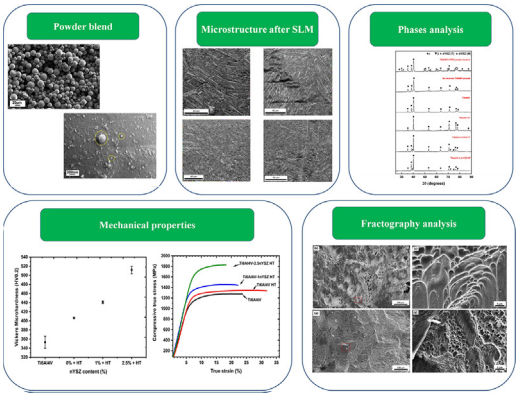

ARTICLE INFO

Article history:
Received 8 March 2019
Received in revised form 22 May 2019
Accepted 31 May 2019
Available online 3 June 2019

Keywords:
Additive manufacturing
Titanium
Selective laser melting
Zirconia
Ti6Al4V
Mechanical properties

ABSTRACT

This study presents the results of selective laser melting (SLM) of Ti6Al4V reinforced with 1% and 2.5% (wt%) nano yttria-stabilized zirconia (nYSZ). The bulk parts showed a very high building density which means that the melting parameters were optimal. X-ray diffraction analysis confirmed the existence of a near-alpha microstructure. No change in grains shape was noticed after the addition of nYSZ, columnar and lamellar grains remained present. The microhardness of Ti6Al4V was greatly enhanced from 340 HV to 511 HV after the addition of nYSZ which is the highest recorded value so far. The maximum values of yield stress and compressive strengths were 1302 MPa and 1751 MPa, respectively, compared to 840 MPa and 1250 MPa, respectively, for the SLMed Ti6Al4V.

1. Introduction

For the past few decades, there has been a huge demand for light weight and strong materials in the aerospace industries. Al, Ti and Mg - based alloys have been widely attractive in such applications due to

* Corresponding author.
E-mail address: dirras@univ-paris13.fr (G. Dirras).

https://doi.org/10.1016/j.matdes.2019.107909

light weight, good machinability and energy efficiency/low power consumption. Nevertheless, despite possessing such a wide range of unique properties, Al-based and Mg-based alloys do not completely satisfy the needed requirements in which the parts are also required to resist high thermal and mechanical stresses. Indeed, these alloys suffer from a noticeable decrease in their mechanical properties from 200 °C [1,2], which strongly limits their use for critical components in the automotive and aerospace sectors. In order to withstand these harsh environment and loadings, light metal matrix (MMC) are called for. In such materials, a light metal matrix is reinforced with ceramic particles at different scales. Titanium strengthened with ceramic particles are the best candidates so far to extend the working temperature of titanium alloys in aeronautical components (as blades in a gas turbine) up to 500 °C. Different reinforcements such as TiC, TiB, B4C [3] and SiC [4] have been added to the titanium matrix to create reinforced titanium matrix in order to improve the tensile strength, shear strength, hardness, and wear resistance. These MMC are made by conventional or vacuum-aided casting techniques [5] or by powder metallurgy [6]. However, these traditional manufacturing processes showed shortcomings such that long manufacture cycle time, high energy consumption, high reinforcement agglomeration [7]. The new layer additive manufacturing (AM) techniques – where a digital 3D data design is used to directly build up a bulk specimen in a layer-by-layer process following deposition, melting, fusion and binding of the successive material layers offer an alternative solution to better enhance the strength, hardness and the fatigue endurance [8] of titanium made aeronautic parts. Additional advantages of AM are: building parts with complex geometries, rapid prototyping, and faster market introduction of new products [9]. Several works are also carried out to enhance the mechanical properties of titanium made parts via the incorporation of reinforcements into the matrix such as B4C, TiC [10] TiB [11] and SiC [12]. However, a tremendous decrease is noticed in ductility due to the melting process and the reinforcement choice. On the other hand, Titanium matrix has never been yet reinforced with yttria-stabilized zirconia nanoparticles (nYSZ) in order to create zirconia reinforced titanium metal matrix (nTMC) processed via AM. YSZ possesses a higher chemical affinity towards titanium [13], a higher fracture toughness over conventional ceramics [14] which makes it the best candidate for titanium.

Therefore, the goal of this work is to investigate for the first time the effect of nYSZ powder addition, on the microstructure and mechanical properties of a Ti6Al4V alloy manufactured via selective laser melting (SLM).

2. Material and experimental methods

2.1. Starting material and SLM process

Ti6Al4V reinforced by 1% and 2.5% nYSZ were fabricated by mixing Ti6Al4V and nYSZ powders and melted using SLM. The Ti6Al4V particle size distribution was measured using SEM and analyzed using ImageJ software (See data in brief document). The Ti6Al4V nominal chemical composition is listed in Table 1. The nYSZ powder is a 3%mol yttria-stabilized tetragonal zirconia with an average particle size of 40 nm (Data provided by USnano, USA). Its chemical composition is listed in Table 2. The powder blend is commercially named ZTi-Powder®. The protocol and melting process was developed and carried out by Z3DLAB company, Paris-France. 8 rotation axis blender (Turbula® T2F) was used with 6 h of mixing time, followed by 10 min pause during each hour. The SLM melting process parameters were used: power 200 W; exposure 100 μs; hatch spacing 80 μm; point distance 65 μm; layer thickness 30 μm and a chess scanning strategy in order to create parallelepiped parts having dimensions of about $10 \times 5 \times 5$ mm^3.

Table 1
Chemical composition of the Ti6Al4V powder in accordance with ASTM F2924.

Element	Ti	Al	V	O	C	N	H	Fe
Weight (%)	Bal	6.2	4.0	0.07	0.01	0.02	0.002	0.14

Table 2
Chemical composition of the 3%mol yttria stabilized tetragonal zirconia nanopowder.

Element	ZrO2	Al	Mg	Si	Ca	S	Nb
Content (ppm)	Bal	20	65	102	75	165	119

2.2. Heat treatment and microstructure observation

The fabricated parts were named as follows: (1) As built Ti6Al4V: Ti6Al4V, (2) Stress relieved Ti6Al4V: Ti6Al4V HT, (3) Stress relieved Ti6Al4V reinforced with 1% of nYSZ: Ti6Al4V-1nYSZ HT, (4) Stress relieved Ti6Al4V reinforced with 2.5% of nYSZ: Ti6Al4V-2.5nYSZ HT. The heat treatment was performed according to AMS 2801 standard (600 °C/2 h in argon protected furnace). Specimens were cut from each part and characterized by X-ray Diffraction to determine the evolution of the constituent phases. The specimens were polished using the following protocol: mechanical polishing with 600–800–1000-1200-2400 and 4000 grids SiC papers, followed by mirror polishing using nano silica solution (OPS) and etching using the Kroll reagent. An optical microscope (ZEISS) and a scanning electron microscope (MEB FEG SUPRA 40VP-ZEISS) were used to characterize the microstructures of the samples. Electron backscatter diffraction (EBSD) investigations were further carried out on electropolished specimens using A3 solution provided by Struers A/S at room temperature.

2.3. Mechanical properties and residual stress measurements

Microhardness tests were conducted according to ASTM E384 standard with a microhardness tester (DuraScan) at a load of 200 gf and a dwell time of 15 s. Ten indentations were achieved on both sides (Building direction plane hereafter: XOZ and scanning direction plane hereafter: XOY) of each part. The distance between indentations was kept higher than 80 μm. Compression tests were performed at room temperature, at a strain rate of 10^{-3} s^{-1} according to ASTM E9 standard. The residual stresses were evaluated using a model developed by Carlsson et al. 2001 [15,16] based on density measurements and microhardness data.

2.4. Density and porosity measurements

Density and porosity measurements were performed for all parts using Archimedes method according to ASTM B962 standards after supports elimination.

3. Results and discussion

3.1. X-ray diffraction analysis (XRD)

The phase analysis of all specimens was determined by XRD with ($14° < 2\theta < 105°$ and $\Delta 2\theta = 0.03°$), using Cu Kαl ($\lambda = 0.154056$ nm) radiation source with an INEL Equinox 1000 X-ray diffractometer. XRD characterization was performed by using two software: MATCH [17] was used for phase identification and Maud (Material Analysis Using Diffraction) [18] to perform Rietveld refinement analysis.

According to XRD patterns shown in Fig. 1, the as received Ti6Al4V powder is essentially composed of Titanium α phase. The addition of nYSZ to the as-received Ti6Al4V powder showed the appearance of a mixture of Titanium α, monoclinic and tetragonal nYSZ as it is seen in the powder mixture of Ti6Al4V and 2.5% nYSZ pattern (see data in brief [19]). The as-built Ti6Al4V showed a mostly α phase. Ti6Al4V HT has mostly α phase. XRD line profiles of Ti6Al4V HT are shifted towards lower angles compared to the as-received Ti6Al4V powder which might be an indication of stress relief effect. According to the Bragg formula, an

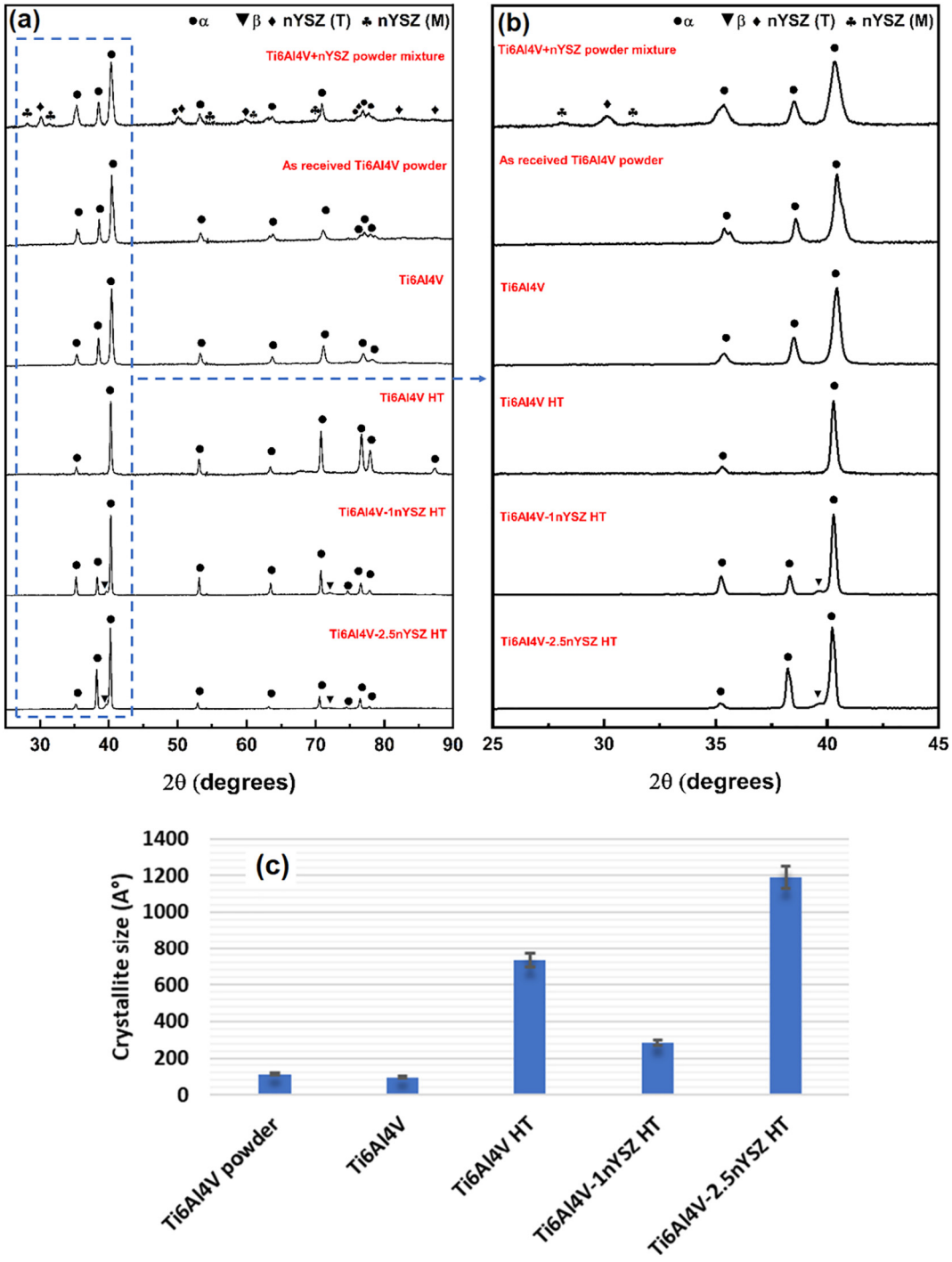

Fig. 1. (a) XRD patterns of the as-received powders and melted parts (α: ●), (β: ▼), (T: Tetragonal ♦ and M: Monoclinic ♣). (b) Is an enlarged area of 2θ = [25°-45°]. (c) Changes in the crystallite sizes of all materials.

increase in the inter-planar spacing results in lower diffraction angles. It was observed by Boyer et al. [20] that when Ti6Al4V is heated up to 800 °C, vanadium phase atoms are rejected from α phase and lattice parameters are changed. XRD patterns of Ti6Al4V-1nYSZ HT and Ti6Al4V-2.5nYSZ HT show also the presence of α phase. The addition of 1% and 2.5% of nYSZ partially stabilized the β phase of Ti6Al4V. According to Rietveld refinement analysis, β phase volume fraction of 1% and 2.5% of nYSZ addition to Ti6Al4V were found to be 10.33% ± 0.57% and 14.24% ± 1.07% respectively (see data in brief [19]), the appearance of β phase could be attributed to the fact that zirconia played the role of a β stabilizer [21]. It is also observed that the addition of nYSZ also shifted the α and β peaks of the melted parts towards lower angles which mean that the introduction of nYSZ into the Ti6Al4V matrix results in lattice distortion. One can notice that nYSZ particles seems to be undetected via XRD after melting. These findings indicate a change in the lattice structure of Ti6Al4V after melting, in line with a previous report [22].

3.2. Lattice parameters

The as-received Ti6Al4V powder lattice parameters *a* and *c* of the HCP phase are measured to be 2.9260 ± 0.0003 Å and 4.6615 ± 0.0005 Å respectively. After melting by SLM, the as built Ti6Al4V lattice parameters *a* and *c* were found to be 2.9380 ± 0.0008 Å and 4.6710 ±

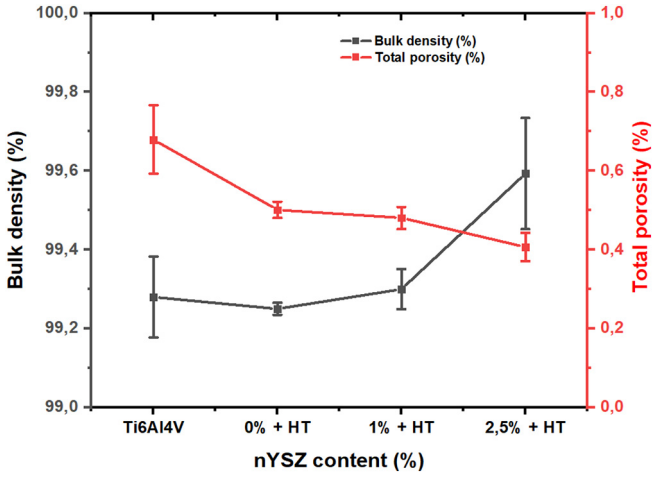

Fig. 2. Effect of nYSZ addition over density and porosity measurements of Ti6Al4V (Ti6Al4V as built), Ti6Al4V HT (0% + HT), Ti6Al4V-1nYSZ HT (1% + HT), and Ti6Al4V-2.5nYSZ HT (2.5% + HT).

0.0005 Å, being thus in agreement with the values of 2.931 Å for *a* and 4.681 Å for *c* of Ti6Al4V processed via SLM [23]. When heat treated, *a* and *c* parameters yielded values of about 2.9406 ± 0.0001 Å and 4.6950 ± 0.0002 Å, respectively. The addition of 1% and 2.5% of nYSZ further increases the *c* lattice parameter, yielding to 4.700 ± 0.0007 Å and 4.7130 ± 0.0004 Å, respectively while reducing the values of the *a* parameter to 2.9406 ± 0.0003 Å and 2.9353 ± 0.0001 Å respectively. This increase of the *c* lattice parameter was also noticed in β-titanium binary alloys Ti—Nb [24] and Ti—Ta [25] where the lattice parameters increased after an addition up to 5% of β alloying elements, and then decreased after further content increase [26]. The a lattice parameter of the β phase showed a decrease from 3.215 ± 0.0029 Å to 3.200 ± 0.0026 Å after 1% and 2.5% nYSZ respectively. According to the obtained results Fig. 1(c), one can notice that the crystallite size of Ti6Al4V HT was increased after heat treatment. However, a significant increase in the crystallite size after the addition of 2.5% of nYSZ compared to 1% of nYSZ, this increase in crystallite size is a sign of defaults reduction.

3.3. Density and porosity measurements

According to Fig. 2, all parts showed high mass density (99.33 to 99.60%). This has also been observed in other studies stating reinforced and heat-treated titanium [23,27]. Adding up to 2.5% of nYSZ has greatly enhanced the density of Ti6Al4V as it can be noticed from Fig. 2. The highest pore content was found in Ti6Al4V (0.68%); this could be due to the small amount of partially melted spherical powder particles [28].

3.4. Microstructural characterization

3.4.1. Powder mixture characterization

Fig. 3 depicts the morphologies of the as-received Ti6Al4V, nYSZ, and the Ti6Al4V + nYSZ powder blend. As it can be seen in Fig. 3(a) and Fig. 3(b) that the as received Ti6Al4V powders exhibit a spherical morphology and nYSZ is in small agglomerates, respectively. It is also seen that the nYSZ particles are attached homogeneously to the surface of Ti6Al4V particles as shown by Fig. 3(c) and (d). Estimation of powder size distribution was made using ImageJ software and the result showed an average powder size of about 25 μm (see data in brief [19]).

3.4.2. Energy-dispersive X-ray spectroscopy analysis (EDX)

In order to investigate the homogeneity of the mixture, an EDX analysis was carried out on the mixed powders under the following working parameters: operating voltage, probe current and deriving time during the data collection were configured at 10 kV, 0.1 nA and 1 h respectively. A scanning area of about 110 × 110 μm^2 was chosen randomly on a powder mixture of Ti6Al4V and 2.5% of nYSZ (Fig. 4(a)). Fig. 4(b, c, d) represents the chemical mapping of titanium zirconium and oxygen respectively. Obviously, titanium is predominant; both zirconium and oxygen are well distributed in the mixture, Oxygen seems to be found in almost the same regions of zirconium. Based on these observations

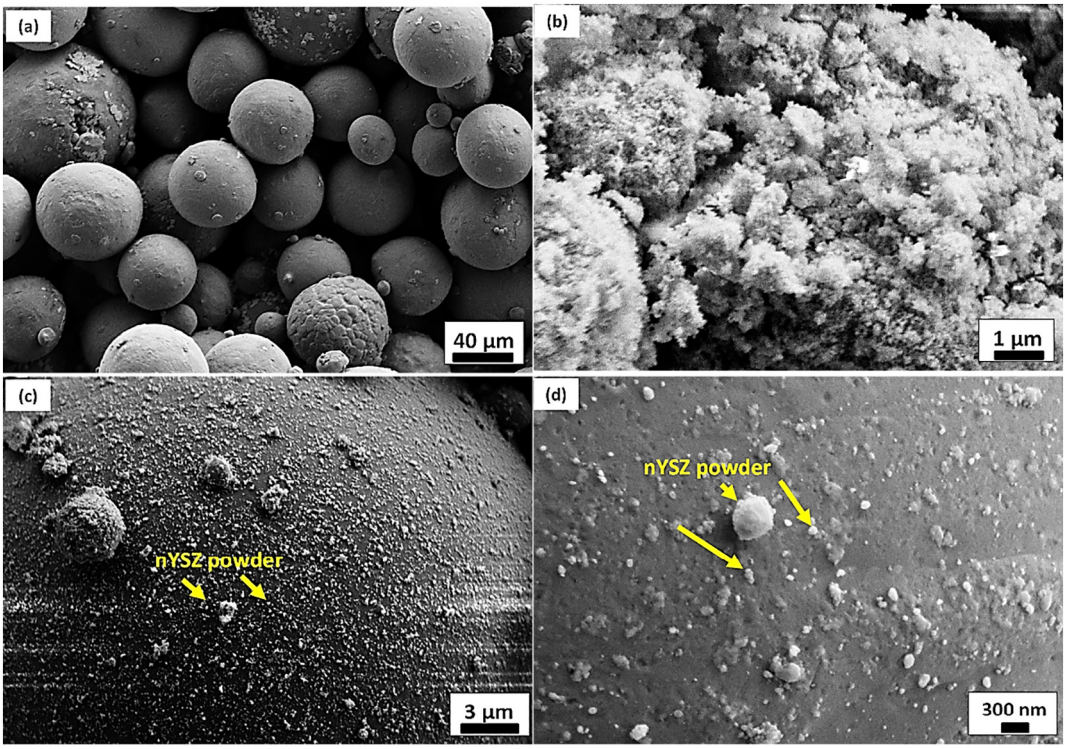

Fig. 3. Particle shape morphology of the starting powders: (a) Ti6Al4V, (b) nYSZ, (c), (d) Ti6Al4V + nYSZ powder blend.

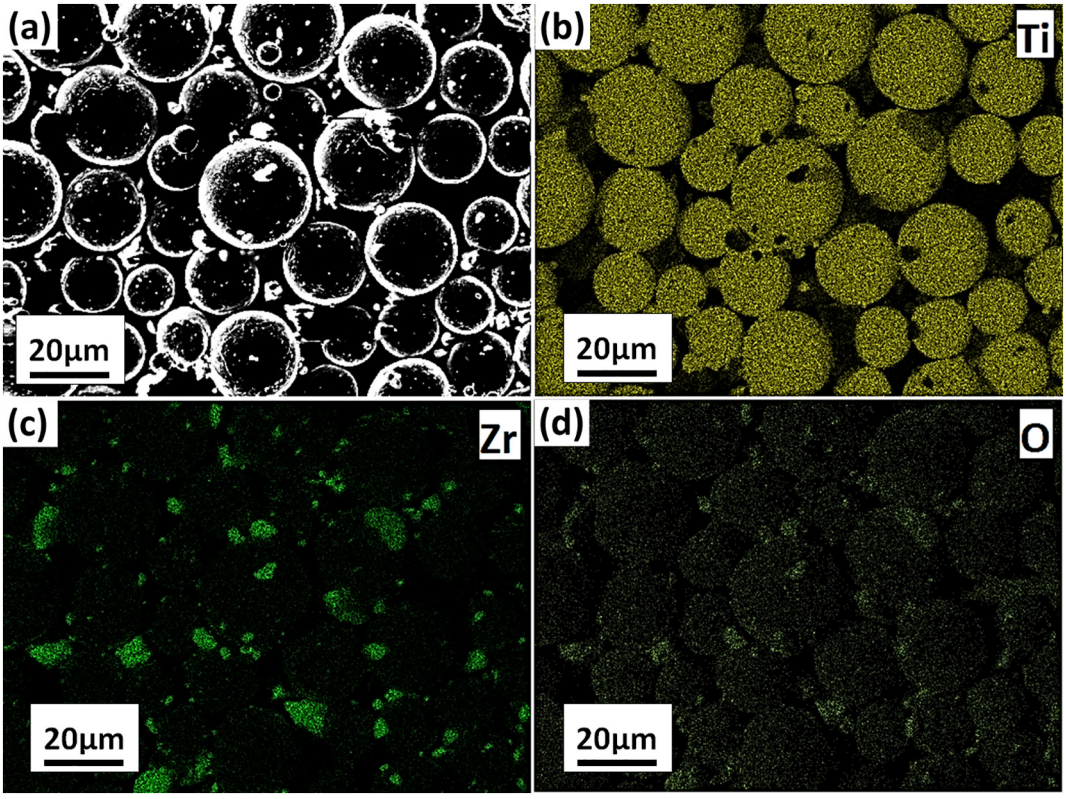

Fig. 4. EDX data of Ti6Al4V + nYSZ powder mixture, analysis performed over several powder grains surface showing a mapping of Ti, Zr and O well distributed and enveloping a Ti6Al4V powder grain. (a): Ti6Al4V+ nYSZ powder mixture, (b): Titanium, (c): Zirconium and (d): Oxygen.

it can be concluded that the mixing protocol results in a homogeneous distribution of nYSZ on Ti6Al4V particles. Some regions contain, however, much more zirconium and oxygen which can be noticed by the color high intensity, which is due to the presence of surface irregularities of Ti6Al4V spherical grains and cavities which are considered as nanopowder capsules. As a result, the nYSZ nanopowder cohesion to Ti6Al4V grains is well ensured.

3.4.3. Bulk parts characterization

SEM images of (XOZ) plan in Fig. 5(a–d), show the presence of lamellar α and of prior β grain boundaries (white dotted lines) that can be noticed in all parts, in accordance with the available literature [29–31]. Prior columnar β grains are about 20 to 50 μm in width for all specimens. According to recent studies, the growth rate of the α lamellar grains depends on the cooling rate [32], which is slightly higher on (XOZ) compared to (XOY) planes as it was described by Awd et al. [33]. This information could help to explain why the microhardness in the (XOZ) plane is higher than that of the (XOY) plane. Fig. 5(e-h) shows the (XOZ) plane microstructure of Ti6Al4V, Ti6Al4V HT, Ti6Al4V-1nYSZ HT and Ti6Al4V-2.5nYSZ HT, respectively using backscattered electrons at higher magnification. It can be noticed that Ti6Al4V presents larger α grains compared to the others. Adding nYSZ to Ti6Al4V further decreased the average grain size. As a result, a fine microstructure was obtained. EBSD analysis (see data in brief [19]) showed that the average length of α grains in Ti6Al4V, Ti6Al4V HT, Ti6Al4V-1nYSZ HT and Ti6Al4V-2.5nYSZ HT is equal to 2.69 μm ± 1.06 μm, 2,49 ± 0.97 μm, 2.47 ± 1 μm and 1.87 ± 0.7 μm, respectively. The average width of α grains was estimated to be 0.72 μm ± 0.11 μm, 0.72 μm ± 0.10 μm, 0.74 μm ± 0.10 μm and 0.63 μm ± 0.09 μm. respectively. The aspect ratio of the parts was calculated and plotted in data in brief document, also confirmed the reduction in α grains aspect ratio after heat treatment and nYSZ addition, this is a sign of change in the ellipsoidal shape of the grains (See data in brief [19]). The reduction in grain size could play a major role in impeding dislocation displacement [34] and give rise to a Hall-Petch-like strengthening mechanism [35,36]. Also, introducing nYSZ into a Ti6Al4V matrix while ensuring a good homogeneity of the powder blend, will create a nYSZ oxide dispersion strengthened (ODS) alloy.

3.5. Mechanical properties

3.5.1. Microhardness tests

According to Fig. 6, which represents the average microhardness values obtained from both planes, Ti6Al4V presents a microhardness of 350 HV which is slightly higher than that of conventional annealed Ti6Al4V (341 HV) [37]. The performed heat treatment increased further microhardness to 406 HV.

This increase in the Ti6Al4V HT microhardness could be attributed to the reduction of the α grain size [23]. The addition of 1% and 2.5% of nYSZ improve, further, the microhardness to 441 and 512 HV, respectively. Together with optimized SLM melting parameters that also reduce the porosity [38] and the addition 2.5% of nYSZ thus results in the elaboration of a homogenous oxide dispersion strengthening alloy (ODS) with exceptional mechanical properties via a processing route that is easier to implement than conventional methods usually used for these materials [37]. In addition, it has been reported that the stronger the particle-matrix bond, the higher the Vickers hardness [39].

3.5.2. Microhardness anisotropy behavior

In order to evaluate the anisotropy of the parts, a HDR (microhardness difference ratio) is calculated as [40,41]:

$$\mathrm{HDR}\ (\%) = \frac{\mathrm{HV}_{(\mathrm{XOZ})} - \mathrm{HV}_{(\mathrm{XOY})}}{\mathrm{HV}_{(\mathrm{XOY})}}$$

where $\mathrm{HV}_{(\mathrm{XOY})}$ and $\mathrm{HV}_{(\mathrm{XOZ})}$ are the average microhardness values measured on the (XOY) and (XOZ) planes, respectively.

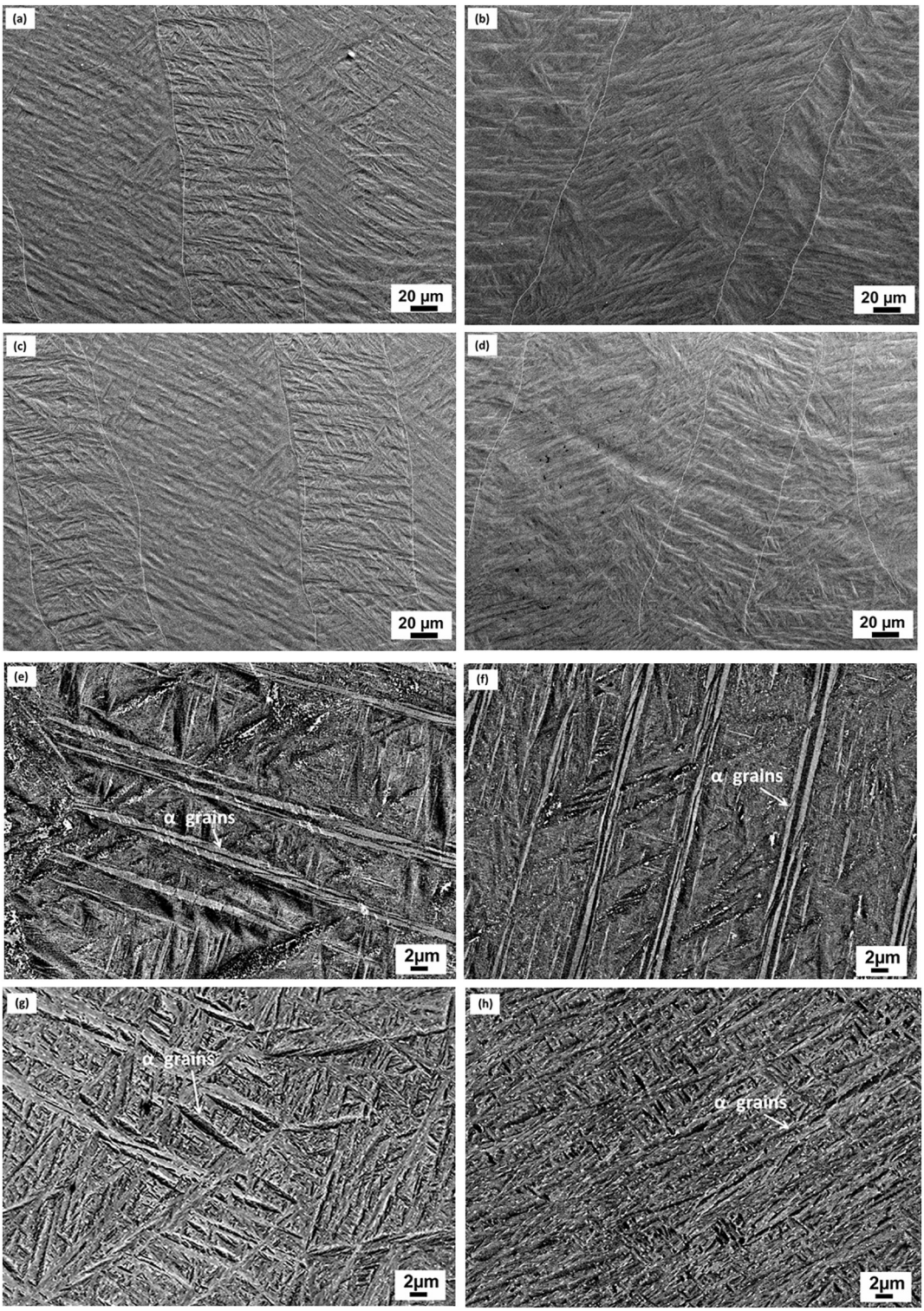

Fig. 5. SEM images of bulk materials (a,e) Ti6Al4V, (b,f) Ti6Al4V HT, (c,g) Ti6Al4V-1nYSZ HT and (d,h) Ti6Al4V-2.5nYSZ HT, showing typical columnar grains of Ti6Al4V processed by SLM (a-d) and a fine microstructure of α lamellar grains(e-h). (White dotted lines are to show prior β grain boundaries.)

It can be observed according to Table 3, that the microhardness values of Ti6Al4V, Ti6Al4V HT, Ti6Al4V-1nYSZ HT and Ti6Al4V-2.5nYSZ HT are slightly higher on the (XOZ) plane than on the (XOY) plane by 7.84, 0.59, 1.27 and 3.29% respectively. This anisotropy could be due to cooling rate difference between the bottom and the upper zones of manufactured parts as already reported by Das et al. [42] which recorded a cooling rate increase from 10^3 to 10^8 K/s for Ti6Al4V manufactured via SLM along the Z axis.

3.5.3. Residual stress nature (compressive or tensile?)

In order to investigate the nature of residual stresses after parts manufacturing and annealing, the model proposed by Carlsson [15,16]

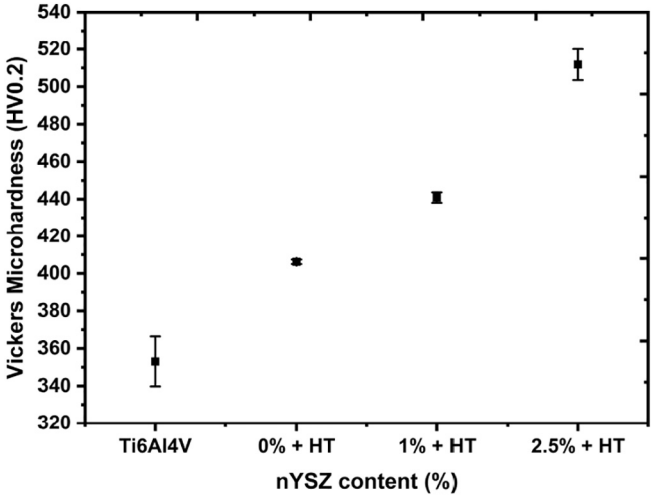

Fig. 6. Effect of nYSZ addition on the average Vickers microhardness of Ti6Al4V processed by SLM. Ti6Al4V (Ti6Al4V as built), Ti6Al4V HT (0% + HT), Ti6Al4V-1nYSZ HT (1% + HT) and Ti6Al4V-2.5nYSZ HT (2.5% + HT).

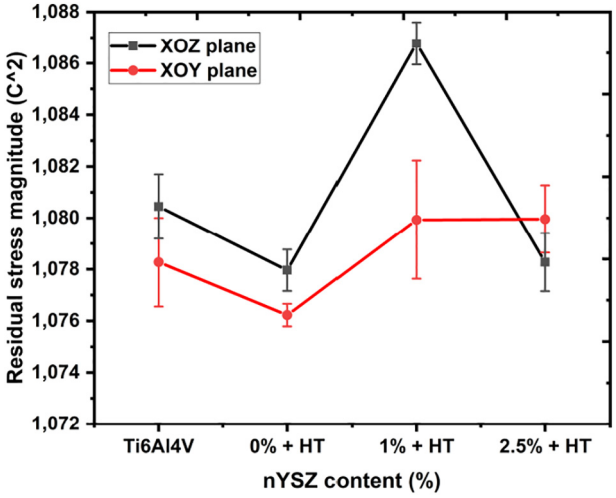

Fig. 7. Influence of heat treatment and nYSZ addition on the residual stress magnitude (C^2) obtained from (XOY) and (XOZ) planes of the build parts: Ti6Al4V (Ti6Al4V as built), Ti6Al4V HT (0% + HT), Ti6Al4V-1nYSZ HT (1% + HT) and Ti6Al4V-2.5nYSZ HT (2.5% + HT).

was employed. Since it was already satisfactorily used to investigate alloys manufactured either via laser forming or additive manufacturing [40,41,43]. Carlsson model uses data obtained from microhardness experiments in order to calculate the so-called residual stress magnitude (C^2), characterized by the ratio of the real projected contact area (A_{real}) to the nominal projected contact area (A_{nom}). C^2 equal to 1 means that all residual stresses are eliminated whereas when C^2 is >1 means that compressive stresses exist within the material resulting into a pilling up behavior on the microhardness imprint and $C^2 < 1$ implies the existence of tensile stresses resulting in a sinking behavior of the microhardness imprints. The results of C^2 calculations on both (XOY) and (XOZ) planes are provided in Fig. 7.

Stress measurements can be related to the size of the contact area. In Vickers test, it is assumed that elastic recovery (spring back) does not occur when the load is removed according to Carlsson et al. 2000 [15,16]. To date, the distribution of residual thermal stresses during SLM has been studied by many researchers by means of neutron diffraction [44] or holes drilling [45]. However, many of these methods are complex and time consuming [41].

It can be seen from Fig. 7 that the C^2 is higher than 1 for both (XOY) and (XOZ) planes, which means that a small amount of residual compressive stresses still exists in all specimens. The lowest value of C^2 is found for the Ti6Al4V HT which thus contains fewer residual stresses than other parts. Adding 1% nYSZ slightly increased (see Fig. 7) the residual stress magnitude and then reduced for an addition of 2.5% nYSZ. Other studies have confirmed that most of additive manufactured parts present residual compressive stresses even after stress annealing [43]. Since that C^2 is higher than 1 for all parts, the model suggests that the microhardness imprints of all specimens should present a piling up behavior, which is indeed confirmed in Fig. 8.

Table 3
Average microhardness values on both (XOY) and (XOZ) planes and associated difference ratio (HDR %).

	HV $_{(XOY)}$	HV $_{(XOZ)}$	HDR (%)
Ti6Al4V	339.80 ± 11.7	366.46 ± 7.3	7.84
Ti6Al4V HT	404.96 ± 6.15	407.37 ± 6.5	0.59
Ti6Al4V-1nYSZ HT	438.14 ± 6.3	443.70 ± 8.7	1.27
Ti6Al4V-2.5nYSZ HT	503.52 ± 9.7	520.10 ± 16.7	3.29

3.5.4. Compression test results

The compression tests were performed at room temperature at a strain rate of 0.001 s^{-1} using a conventional machine, type MTS (model: 20/M-10KN). On average, three tests were conducted per sample. The compression axis was perpendicular with the building direction of all samples. The results are shown in Fig. 9. Because no extensometer was used, sets of both true stress – true strain and true stress – true plastic strain are displayed in Fig. 9(a) and (b), respectively. For the latter, plastic deformation (ε_p) was calculated as described in the Data in Brief associated with the present work [19]. In the following, we will discuss the effect of composition and heat treatment on the macroscopic mechanical characteristics

3.5.4.1 Effect of the composition the elastic behavior

Fig. 9(a) indicates the effect of the addition of nYSZ on the evolution of the elastic modulus. Indeed, it can be observed that the reinforced materials have an increase in the elastic slope of about 6% compared to as-built or heat-treated materials that do not contain reinforcements. This effect is expected and is due by the fact that the nYSZ particles will modify the intensity of the atomic bonds and thus contribute to the increase of the elastic modulus. In the absence of an extensometer, the actual values of the elastic moduli for both set of alloys cannot be computed from the curves shown in Fig. 9(a). We measured Young's moduli of as-built Ti6Al4V and Ti6Al4V-2.5nYSZ-HT by sound wave propagation techniques [46]. These experiments gave 108 GPa and 115 GPa for the as-built and the reinforced alloys, respectively.

3.5.4.2 Effect of composition on the strength and the plastic deformation

The effect of the composition is visualized by comparing the as-built material to the other two reinforced materials with 1% and 2.5% of nYSZ. The macroscopic data are presented and summarized in Table 4 (which also compares the literature data). Compared to the as-built material, an increase of the yield strength of the order of 15% and 36% can be observed after addition of 1% and 2.5% of nYSZ, respectively. At the same time, the relative hardening calculated here as $n = ((\sigma_{0.2}-\sigma_0)/\sigma_0)$ is also increased (here $\sigma_{0.2}$ is the flow stress at 0.2% offset and σ_0 is the yield strength). It is of the order of 11% for the as-built, and 15% for the reinforced materials. Most probably, the dispersed nYSZ particles oxides impede dislocations' movement at the early stage of plastic deformation.

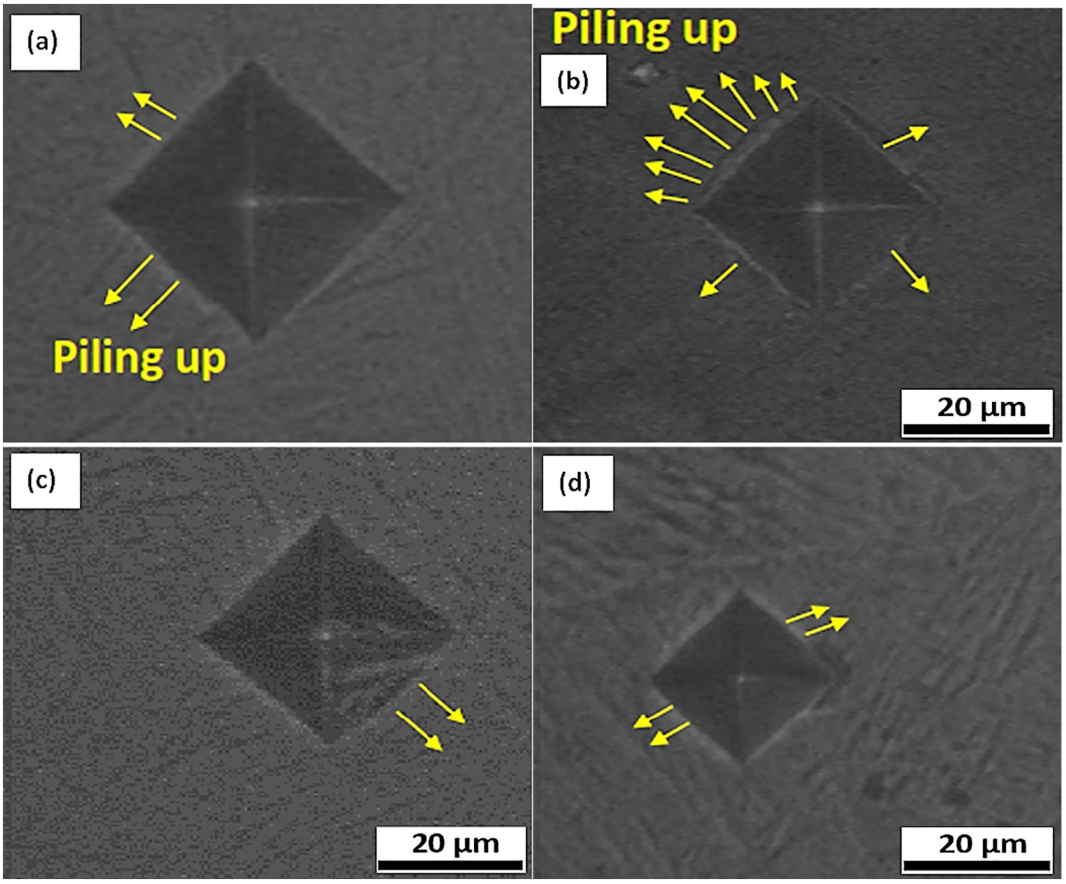

Fig. 8. Microhardness imprints of (a) Ti6Al4V, (b) Ti6Al4V HT, (c) Ti6Al4V-1nYSZ HT and (d) Ti6Al4V-2.5nYSZ HT via optical microscope.

In the same way, it should be noticed that addition of 1% and 2.5% of nYSZ to the Ti6Al4V matrix increases the maximum compressive stress to (1427 ± 80 MPa) and (1751 ± 53 MPa) respectively which is higher than that recorded for Ti6Al4V reinforced by SiC nanopowder [38]. These values are higher than that recorded for conventional annealed Ti6Al4V [37] or Ti-5%TiB by SLM [27].

Nevertheless, the effect of a refinement of the microstructure on the macroscopic mechanical behavior cannot be ruled out. Indeed, as shown by the EBSD grain size map of Fig. 6 and Fig. 7 of the Data in Brief, the aspect ratio of the alpha lamellae decreases continuously with the heat treatment and the addition of nYSZ (see also Table 1 of the Data in Brief), going from 3.73 ± 0.11 down to 2.96 ± 0.09. Thus, the finer the microstructure, the more dependence of the flow stress according to the Hall-Petch law is expected. But in such a complex microstructure, the different effects are difficult to separate.

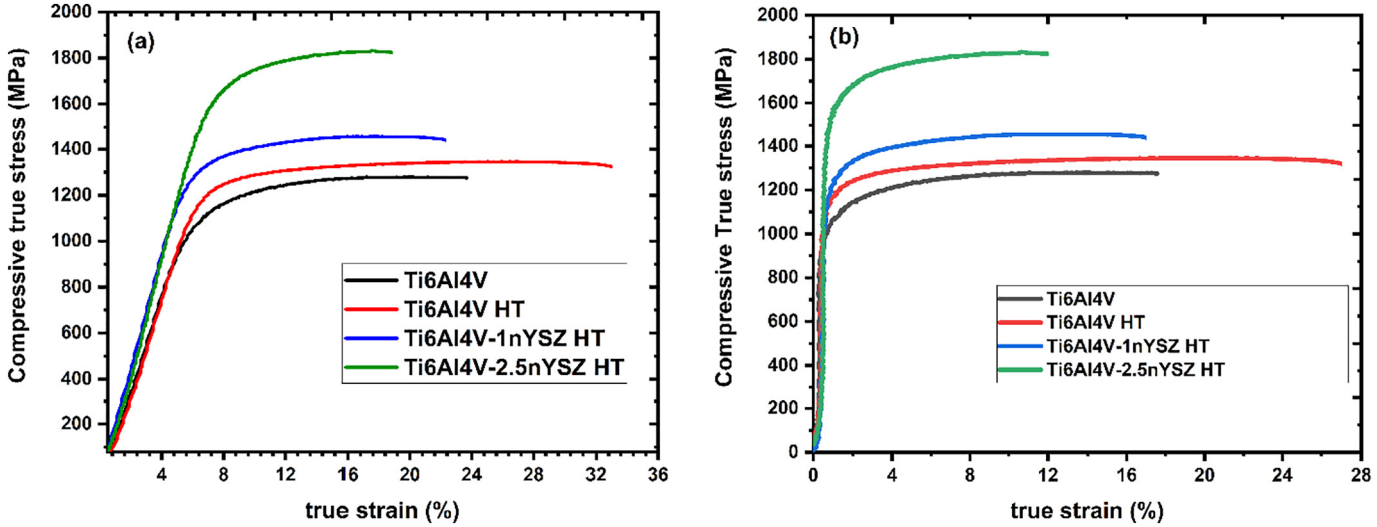

Fig. 9. (a) Compression true Stress – Strain and (b) and plastic true Stress – Strain curves of Selective laser melted Ti6Al4V, Ti6Al4V HT, Ti6Al4V -1nYSZ HT and Ti6Al4V-2.5nYSZ HT.

Table 4
Compression tests data results for Ti6Al4V and Ti6Al4V reinforced and manufactured via powder bed fusion technology. (USC: Ultimate compression strength, YS: Yield strength, CS: Compression strain).

Material	UCS (MPa)	YS (MPa)	CS (%)	Reference
Ti6Al4V (SLM)	1251 ± 22	840 ± 25	23 ± 1	This study
Ti6Al4V-Gd23 ELI	–	860	35	ASTM F136
Ti6Al4V (EBM)	1114 ± 34	–	–	[47]
Ti6Al4V (SLM)	1198 ± 12	862 ± 53	–	[48]
Ti6Al4V HT (SLM)	1337 ± 10	960 ± 10	33,5 ± 2	This study
Ti6Al4V-1nYSZ HT (SLM)	1427.04 ± 80	1110 ± 80	25 ± 4	This study
Ti6Al4V-2.5nYSZ HT (SLM)	1750.61 ± 53	1301 ± 5	19 ± 2.2	This study
Ti-5%TiB (SLM)	1400	1102	20	[11]

3.5.4.3 Effect of the heat treatment

A comparison of the mechanical behavior of unreinforced materials, namely Ti6AL4V as-built and Ti6Al4V-HT shows a gain in mechanical properties (elastic limit and ductility) in favor of thermally treated alloy. In fact, the elastic limit increases by 17% and the relative hardening is about 15% (11% for the case of as-built material). In addition, the EBSD analysis (Fig. 7 of the Data in Brief) are sharper and the lamellae are thinner. These two results explain the much better observed mechanical resistance, as well as an improved plastic deformation to failure. Indeed, the heat treatment has also been able to eliminate the residual stresses of the as-built state, thus improving the ductility in compression.

When the unreinforced but heat-treated material is compared with the reinforced and thermally treated materials, the latter display a grain of yield strength and mechanical strength, which is detrimental to ductility (Fig. 9(b)). It is observed, however, that the rate of relative hardening is of the same order of magnitude and is around 15%. This result indicates that this initial work-hardening could come more from a Hall-Petch effect than from a dispersion effect of the oxides in the material (ODS) since such a dispersion is not present for the Ti6Al4V-HT counterpart.

Table 4 compares the compression data for the as built and heat-treated Ti6Al4V, Ti6Al4V reinforced and processed via powder bed fusion (PBF), electron beam melting (EBM) and SLM, it can be concluded that our study offers promising results regarding the strengthening of Ti6Al4V matrix via SLM over the existent titanium reinforced. During compression tests, only Ti6Al4V HT and Ti6Al4V-1nYSZ HT were fractured along an angle of 45° to the compression axis. A surface analysis was performed on both specimens (Fig. 10). For Ti6Al4V HT, the surface (Fig. 10(a)) showed some shear-like fracture and displayed mostly elongated dimples (Fig. 10(b)), which is a sign of a ductile fracture. However, Ti6Al4V-1nYSZ HT fractured surface (Fig. 10(c)) presented a combination of river-like surface in addition to dimples but no shear-like surface was noticed (Fig. 10(d)). These observations suggest that the addition of nYSZ has modified the fracture behavior of Ti6Al4V. More investigations are still needed to completely clarify the underlying fracture mechanism.

4. Conclusion

In this study, Ti6Al4V and controlled volume fractions of nYSZ powders were blended and melted via SLM technology. The produced parts showed a very high density of about 99.6%, meaning that the processing parameters were optimal. XRD results showed the presence of mostly α phase (~99%) in the as-built Ti6Al4V specimen and a small amount of β phase with the addition of 1% and 2.5% of nYSZ reinforcement. The grains shape of Ti6Al4V reinforced with nYSZ was typical of Ti6Al4V made by SLM. However, the average length of lamellar α grains was reduced from 2.69 μm to 1.87 μm. The microhardness of the parts was greatly enhanced from 340 HV to almost 511 HV. Residual stress evaluations were performed, and the results showed the existence of compressive type of residual stresses. The compressive strength of nYSZ reinforced Ti6Al4V was enhanced up to 1751 MPa. The ductility of Ti6Al4V was maintained after the addition of 1% of nYSZ. These properties could be very useful in fields like aeronautic, defense, nuclear and petrochemical fields.

Acknowledgements

Authors are grateful to Z3DLAB company and the Association Nationale de la Recherche et de la Technologie (ANRT) for their financial support, through grant N° 2017/0630.

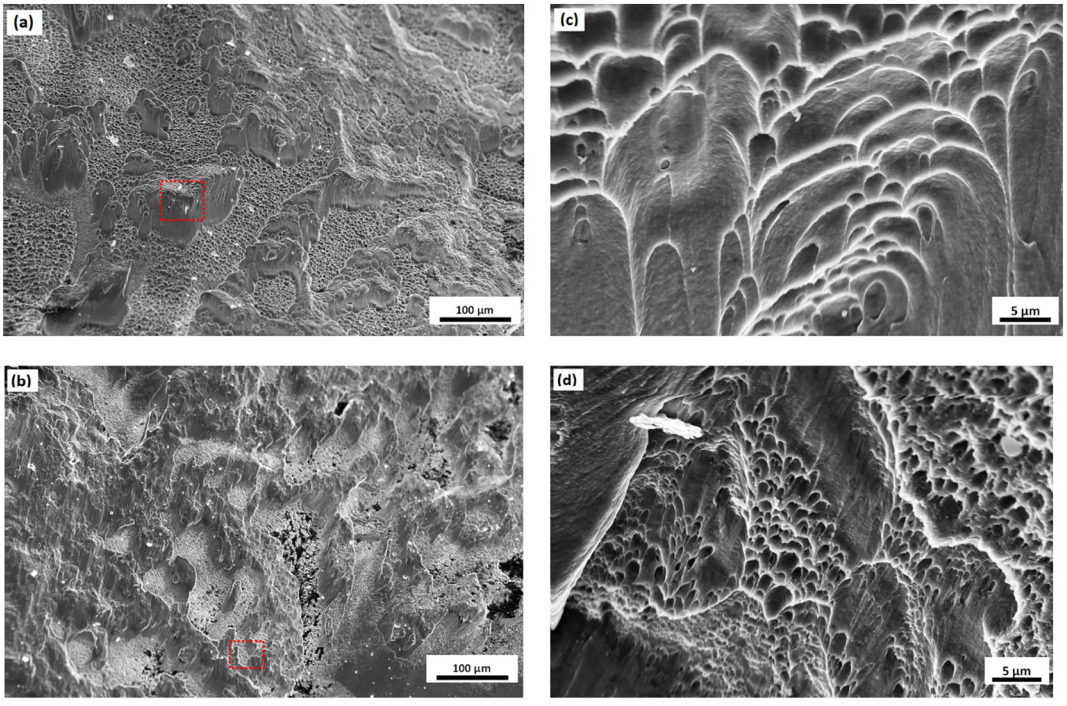

Fig. 10. SEM images of fractured surfaces of the SLM (a) Ti6Al4V HT and (b) Ti6Al4V-1nYSZ HT. (c) and (d) are the magnification of (a) and (b) regions highlighted by dotted rectangles.

References

[1] M.K. Surappa, Aluminium matrix composites: challenges and opportunities, Sadhana 28 (2003) 319–334.
[2] H.E. Friedrich, B.L. Mordike, Magnesium Technology: Metallurgy, Design Data, Applications, Springer, Berlin, New York, 2006.
[3] D.R. Ni, L. Geng, J. Zhang, Z.Z. Zheng, Effect of B4C particle size on microstructure of in situ titanium matrix composites prepared by reactive processing of Ti–B4C system, Scr. Mater. 55 (2006) 429–432.
[4] G. Sivakumar, V. Ananthi, S. Ramanathan, Production and mechanical properties of nano SiC particle reinforced Ti–6Al–4V matrix composite, T Nonferr Metal Soc 27 (2017) 82–90.
[5] L. Xiao, W.J. Lu, J.N. Qin, Y.F. Chen, D. Zhang, M.M. Wang, F. Zhu, B. Ji, Steady state creep of in situ TiB plus La2O3 reinforced high temperature titanium matrix composite, Mater. Sci. Eng. A 499 (2009) 500–506.
[6] M.Y. Koo, J.S. Park, M.K. Park, K.T. Kim, S.H. Hong, Effect of aspect ratios of in situ formed TiB whiskers on the mechanical properties of TiBw/Ti–6Al–4V composites, Scr. Mater. 66 (2012) 487–490.
[7] R. Banerjee, P.C. Collins, A. Genç, H.L. Fraser, Direct laser deposition of in situ Ti–6Al–4V–TiB composites, Mater. Sci. Eng. A 358 (2003) 343–349.
[8] F. Cao, T. Zhang, M.A. Ryder, D.A. Lados, A review of the fatigue properties of additively manufactured Ti-6Al-4V, JOM 70 (2018) 349–357.
[9] H. Fayazfar, M. Salarian, A. Rogalsky, D. Sarker, P. Russo, V. Paserin, E. Toyserkani, A critical review of powder-based additive manufacturing of ferrous alloys: process parameters, microstructure and mechanical properties, Mater. Des. 144 (2018) 98–128.
[10] S. Pouzet, P. Peyre, C. Gorny, O. Castelnau, T. Baudin, F. Brisset, C. Colin, P. Gadaud, Additive layer manufacturing of titanium matrix composites using the direct metal deposition laser process, Mater. Sci. Eng. A 677 (2016) 171–181.
[11] H. Attar, M. Bönisch, M. Calin, L.C. Zhang, K. Zhuravleva, A. Funk, S. Scudino, C. Yang, J. Eckert, Comparative study of microstructures and mechanical properties of in situ Ti–TiB composites produced by selective laser melting, powder metallurgy, and casting technologies, J. Mater. Res. 29 (2014) 1941–1950.
[12] P. Krakhmalev, I. Yadroitsev, Microstructure and properties of intermetallic composite coatings fabricated by selective laser melting of Ti–SiC powder mixtures, Intermetallics 46 (2014) 147–155.
[13] X.B. Zhou, J.T.M. De Hosson, Reactive wetting of liquid metals on ceramic substrates, Acta Mater. 44 (1996) 421–426.
[14] S. Jayalakshmi, M. Gupta, Light Metal Matrix Composites, in: Metallic Amorphous Alloy Reinforcements in Light Metal Matrices, Springer International Publishing, Cham, 2015 7–58.
[15] S. Carlsson, On the determination of residual stress and strain fields by sharp indentation testing. Part i: theoretical and numerical analysis, Acta Mater. 49 (12) (2001) 2179.
[16] S. Carlsson, On the determination of residual stress and strain fields by sharp indentation testing. Part ii: experimental investigation, Acta Mater. 49 (12) (2001) 2193–2203.
[17] Match! Phase Identification From Powder Diffraction, http://www.crystalimpact.com/match/.
[18] L. Lutterotti, S. Matthies, H.R. Wenk, MAUD: A Friendly Java Program for Material Analysis Using Diffraction, IUCr: Newsletter of the CPD 21, 1999 14–15.
[19] Data Related to Phase Analysis, Microstructural Characterization and Mechanical Properties of Additive Manufactured Ti6Al4V Reinforced with Nano Yttria Stabilized Zirconia, 2019 (submitted alongside the present research paper).
[20] R. Boyer, G. Welsch, E.W. Collings, Materials Properties Handbook: Titanium Alloys, ASM International, Ohio, 1994.
[21] B. Zhang, B. Ma, X. Zhang, Q. Zhu, X. Ren, Y. Zhang, X. Qu, J. Yu, J. Yu, Effects of YSZ and nano-ZrO 2 contents on the properties of Ti2448-ZrO 2 biomedical composites fabricated by SPS, Ceram. Int. 44 (2018) 13293–13302.
[22] C. Xia, Z. Zhang, Z. Feng, B. Pan, X. Zhang, M. Ma, R. Liu, Effect of zirconium content on the microstructure and corrosion behavior of Ti-6Al-4V- x Zr alloys, Corros. Sci. 112 (2016) 687–695.
[23] X.-Y. Zhang, G. Fang, S. Leeflang, A.J. Böttger, A.A. Zadpoor, J. Zhou, Effect of subtransus heat treatment on the microstructure and mechanical properties of additively manufactured Ti-6Al-4V alloy, J. Alloys Compd. 735 (2018) 1562–1575.
[24] S. Banumathy, R.K. Mandal, A.K. Singh, Structure of orthorhombic martensitic phase in binary Ti–Nb alloys, J. Appl. Phys. 106 (2009), 093518.
[25] D.E. Huber, Structure and Properties of Titanium Tantalum Alloys for Biocompatibility, PhD Thesis Graduate School of the Ohio State University, 2016.
[26] O. Joris, Diffraction Experiments on Superelastic Beta Titanium Alloys, [dissertation] Imperial College, London, 2015.
[27] H. Attar, M. Bönisch, M. Calin, L.-C. Zhang, S. Scudino, J. Eckert, Selective laser melting of in situ titanium–titanium boride composites: processing, microstructure and mechanical properties, Acta Mater. 76 (2014) 13–22.
[28] S.L. Lu, H.P. Tang, Y.P. Ning, N. Liu, D.H. StJohn, M. Qian, Microstructure and mechanical properties of long Ti-6Al-4V rods additively manufactured by selective electron beam melting out of a deep powder bed and the effect of subsequent hot isostatic pressing, Metall. Mater. Trans. A. 46 (2015) 3824–3834.
[29] B. Vrancken, L. Thijs, J.-P. Kruth, J. Van Humbeeck, Heat treatment of Ti6Al4V produced by selective laser melting: microstructure and mechanical properties, J. Alloys Compd. 541 (2012) 177–185.
[30] H. Ali, H. Ghadbeigi, K. Mumtaz, Effect of scanning strategies on residual stress and mechanical properties of selective laser melted Ti6Al4V, Mater. Sci. Eng. A 712 (2018) 175–187.
[31] T. Vilaro, C. Colin, J.D. Bartout, As-fabricated and heat-treated microstructures of the Ti-6Al-4V alloy processed by selective laser melting, Metall. Mater. Trans. A. 42 (2011) 3190–3199.
[32] J. Yang, H. Yu, J. Yin, M. Gao, Z. Wang, X. Zeng, Formation and control of martensite in Ti-6Al-4V alloy produced by selective laser melting, Mater. Des. 108 (2016) 308–318.
[33] M. Awd, J. Tenkamp, M. Hirtler, S. Siddique, M. Bambach, F. Walther, Comparison of microstructure and mechanical properties of Scalmalloy® produced by selective laser melting and laser metal deposition, Materials 11 (2017) 17.
[34] R.S. Rana, R. Purohit, S. Das, Fabrication and testing of ultrasonically assisted stir cast AA 5083-Sicp composites, Int. J. Eng. Res. Appl. 3 (2013) 386–393.
[35] A.M. Beese, Microstructure and mechanical properties of AM builds, Thermo-Mechanical Modeling of Additive Manufacturing, Elsevier 2018, pp. 81–92.
[36] P. Sirilar, P. Srichandr, Grain refinement of α/β phase Ti–6Al–4V alloy by thermomechanical treatment, Proceedings of the 4th Thailand Materials Science & Technology Conference, Paper M13 2006, pp. 1–3.
[37] ASTM F136 - 13 Standard Specification for Wrought Titanium-6 Aluminum-4 Vanadium Eli (Extra Low Interstitial) Alloy for Surgical Implant Applications (UNS R56401).
[38] G. Sivakumar, V. Ananthi, S. Ramanathan, Production and mechanical properties of nano SiC particle reinforced Ti–6Al–4V matrix composite, T Nonferr Metal Soc 27 (2017) 82–90.
[39] B.S. Murty, S.K. Thakur, B.K. Dhindaw, On the infiltration behavior of Al, Al-Li and Mg melts through SiCp bed, Metall. Mater. Trans. A 31A (2000) 319–325.
[40] X. Wang, Y.K. Chou, A method to estimate residual stress in metal parts made by selective laser melting, Advanced Manufacturing, vol. 2A, ASME, Houston, Texas, USA, 2015.
[41] J. Cao, F. Liu, X. Lin, C. Huang, J. Chen, W. Huang, Effect of overlap rate on recrystallization behaviors of laser solid formed Inconel 718 superalloy, Opt. Laser Technol. 45 (2013) 228–235.
[42] M. Das, V.K. Balla, D. Basu, S. Bose, A. Bandyopadhyay, Laser processing of SiC-particle-reinforced coating on titanium, Scr. Mater. 63 (2010) 438–441.
[43] R. Baskett, Effect of Support Structure Geometry on SLM Induced Residual Stresses in Overhanging Features, PhD Thesis The Faculty of California Polytechnic State University, September 2017.
[44] L. Hehn, C. Zheng, Measurement of residual stresses in Al2O3/Ni laminated composites using an X-ray diffraction technique, J. Mater. Sci. 30 (1995) 1277.
[45] N.J. Rendler, I. Vigness, Hole-drilling strain-gage method of measuring residual stresses: authors indicate that this method permits the magnitudes and principal directions of residual stresses at the hole location to be determined, Exp. Mech. 6 (1966) 577–586.
[46] P. Majumdar, S.B. Singh, M. Chakraborty, Elastic modulus of biomedical titanium alloys by nano-indentation and ultrasonic techniques—a comparative study, Mater. Sci. Eng. A 489 (2008) 419–425.
[47] O.L. Rodriguez, P.G. Allison, W.R. Whittington, H. El Kadiri, O.G. Rivera, M.E. Barkey, Strain rate effect on the tension and compression stress-state asymmetry for electron beam additive manufactured Ti6Al4V, Mater. Sci. Eng. A 713 (2018) 125–133.
[48] S. Zhang, Q. Wei, L. Cheng, S. Li, Y. Shi, Effects of scan line spacing on pore characteristics and mechanical properties of porous Ti6Al4V implants fabricated by selective laser melting, Mater. Des. 63 (2014) 185–193.